Electronic Structure of Small Spherical Metal Shells

Sci. Rep. RITU A41 (1996) pp. 133-140
No. 2, January 1996

Electronic Structure of Small Spherical Metal Shells

Takeshi Inaoka

Department of Materials Science and Technology, Faculty of Engineering, Iwate University, 4-3-5 Ueda, Morioka, Iwate 020, Japan

(Received November 14, 1995)

The ground-state electronic structure of small spherical metal shells is examined on the basis of a model system which consists of valence electrons and a spherical jellium shell (JS). The electron density distribution and the effective one-particle potential are calculated by means of the density functional theory involving the local density approximation (LDA) and the self-interaction correction (SIC). By varying the electron number and the inner radius of the JS under the charge-neutrality condition of the whole system, we closely examine how the electronic structure evolves from a jellium-sphere system to an electron system sharply localized around a spherical surface. By comparing the results in the SIC-LDA scheme with those in the ordinary LDA scheme, we evaluate effects of the SIC especially on energy levels of occupied electron shells.

KEYWORDS: spherical metal shell, electronic structure, jellium model, local-density-functional formalism, self-interaction correction

1. Introduction

Metal coating to small particles forms small spherical metal shells, where electron systems are localized in the radial direction and have the inner and outer surfaces. In such electron systems, surface plasmons occur at the outer and inner surfaces, which interact with each other according to the shell thickness.[1,2] These surface excitations can be observed in photoabsorption spectra.[3,4] In addition, an electron system in a spherical metal shell is intermediate between that in a solid metal sphere and that confined on a spherical surface. This intermediate character is considered to show itself in electronic structures and in electronic excitations. Recently, this subject has been investigated both experimentally[4] and theoretically.[5-10] This subject is also connected with fullerene molecules such as C_{60}[11] whose electronic states are localized around the hollow-cage structure.[12]

The electronic structure of metal spheres has been examined on the basis of a spherical jellium-background model by using the density-functional theory involving the local density approximation (LDA).[13-16] Results of this examination support experimental observations such as the stability of metal clusters at shell-closing electron numbers and the effect of electron shells on the size dependence of the ionization potential.[17,18]

By incorporating the self-interaction correction (SIC)[19] into the ordinary LDA scheme, [20] we can obtain a significant improvement in orbital-energy and total-energy calculations. In the SIC-LDA scheme, we subtract the self-interaction contribution from each of the electrostatic Hartree part and the exchange-correlation part of the effective one-particle potential, such that each occupied orbital does not interact with itself within the LDA framework. Eigenenergies of occupied orbitals in the SIC-LDA scheme closely approximate quasiparticle energies, namely, removal energies including orbital relaxation effects. Accordingly, we can accurately evaluate the ionization potential by the highest energy level of occupied orbitals. Application of the SIC to jellium spheres has proved that the SIC is very effective for precise energy analysis.[16]

The purpose of the present work is to investigate the ground-state electronic structure of small spherical metal shells. By using the SIC-LDA scheme, we calculate the electronic structure of our model system made up of valence electrons and a spherical jellium shell (JS). Fixing the outer radius and the smeared-out ion density of the JS, we change the electron number and the inner radius of the JS at the same time, under the charge-neutrality condition of the whole system. With increase in size of the hollowed-out core, we follow the variation of the electronic structure from a solid jellium sphere to a spherical thin layer. In order to estimate effects of the SIC, we compare the results of the SIC-LDA calculation with those of the ordinary LDA calculation. Details of the present work have already been reported in refs. 7 and 10.

2. Theory

We briefly describe a theoretical framework for the present study. We use the parametrized exchange-correlation (XC) potential[19] obtained from Ceperley and Alder's Monte Carlo calculation.[21] In the following equations, energy and length are measured in the Rydberg unit 13.61 eV and the Bohr radius 0.5292 Å, respectively. We employ spherical polar coordinates and locate the origin at the center of the JS. Our electron systems treated here have no spin polarization. For simplicity, we eliminate spin indices in the following expressions.

Following Perdew and Zunger,[19] we incorporate

the SIC into the ordinary LDA scheme. The effective one-particle potential becomes dependent upon orbital in the SIC-LDA scheme. The ground-state electronic structure can be obtained by solving the following set of equations self-consistently:

$$\left[-\Delta + V_{\mathrm{eff}}{}^{\alpha}(\boldsymbol{r})\right]\psi_{\alpha}(\boldsymbol{r}) = \varepsilon_{\alpha}\psi_{\alpha}(\boldsymbol{r}), \tag{1}$$

$$\rho_{\alpha}(\boldsymbol{r}) = f_{\alpha}|\psi_{\alpha}(\boldsymbol{r})|^2, \tag{2}$$

$$\rho(\boldsymbol{r}) = 2\sum_{\alpha}\rho_{\alpha}(\boldsymbol{r}), \tag{3}$$

$$V_{\mathrm{eff}}{}^{\alpha}(\boldsymbol{r}) = V_{\mathrm{H}}{}^{\alpha}(\boldsymbol{r}) + V_{\mathrm{xc}}{}^{\alpha}(\boldsymbol{r}), \tag{4}$$

where two components of $V_{\mathrm{eff}}{}^{\alpha}$ are constructed by

$$V_{\mathrm{H}}{}^{\alpha}(\boldsymbol{r}) = V_{\mathrm{H}}{}^{(0)}(\boldsymbol{r}) - 2\int \mathrm{d}^3\boldsymbol{r}'\frac{\rho_{\alpha}(\boldsymbol{r}')}{|\boldsymbol{r}-\boldsymbol{r}'|}$$

$$= V_{\mathrm{JS}}(\boldsymbol{r}) + 2\int \mathrm{d}^3\boldsymbol{r}'\frac{\rho(\boldsymbol{r}')}{|\boldsymbol{r}-\boldsymbol{r}'|} - 2\int \mathrm{d}^3\boldsymbol{r}'\frac{\rho_{\alpha}(\boldsymbol{r}')}{|\boldsymbol{r}-\boldsymbol{r}'|}, \tag{5}$$

and

$$V_{\mathrm{xc}}{}^{\alpha}(\boldsymbol{r}) = V_{\mathrm{xc}}{}^{(0)}[\rho(\boldsymbol{r})] - V_{\mathrm{xc}}{}^{\mathrm{P}}[\rho_{\alpha}(\boldsymbol{r})]. \tag{6}$$

In these equations, $\psi\alpha(\boldsymbol{r})$ and $\varepsilon\alpha$ denote the Kohn-Sham single-particle eigenfunction and eigenenergy for orbital α, and $f\alpha(=1$ or $0)$ and $\rho\alpha(\boldsymbol{r})$ signify, respectively, the occupation number and the orbital density of a state with orbital α and up- or down-spin. The density $\rho(\boldsymbol{r})$ is the electron number density including both spin orientations. In eq. (5), $V_{\mathrm{JS}}(\boldsymbol{r})$ represents the electrostatic potential produced by a uniform positive-charge distribution of the JS. In eq. (6), $V_{\mathrm{xc}}{}^{(0)}[\rho]$ denotes the XC potential for an unpolarized electron gas with density ρ, while $V_{\mathrm{xc}}{}^{\mathrm{P}}[\rho\alpha]$ signifies the XC potential for a fully polarized electron gas with density ρ_{α}. The electrostatic Hartree and XC potentials $V_{\mathrm{H}}{}^{\alpha}$ and $V_{\mathrm{xc}}{}^{\alpha}$ are, respectively, obtained from $V_{\mathrm{H}}{}^{(0)}$ and $V_{\mathrm{xc}}{}^{(0)}$ by subtracting the electrostatic and the XC contribution of the relevant orbital density ρ_{α} The eigenfunction and the eigenenergy for each orbital are given by the solution for the effective potential which does not include the self-interaction contribution in each of its electrostatic and XC components.

Our calculations are concerned with closed-shell configurations. Each orbital is specified by n, l, and m, namely, the radial, the orbital-angular-momentum and the magnetic quantum numbers. Energy eigenstates for $l>0$ are degenerate with respect to m, and a set of $2(2l+1)$-fold degenerate states including spin form an electron shell, which is labeled by n and l. When $l>0$, before building up $V_{\mathrm{eff}}{}^{\alpha}$ by eqs. (4)-(6), we spherically the orbital density $\rho_{\alpha}(\boldsymbol{r})$ by averaging it over m.

In order to analyze the thickness dependence of each eigenenergy, we decompose the eigenenergy $\varepsilon\alpha$ into the radial kinetic energy $\varepsilon_{\mathrm{rk},\alpha}$, the centrifugal potential energy $\varepsilon_{\mathrm{cp},\alpha}$, the electrostatic Hartree potential energy $\varepsilon_{\mathrm{H},\alpha}$ and the XC potential energy $\varepsilon_{\mathrm{xc},\alpha}$:

$$\varepsilon_{\alpha} = \varepsilon_{\mathrm{rk},\alpha} + \varepsilon_{\mathrm{cp},\alpha} + \varepsilon_{\mathrm{H},\alpha} + \varepsilon_{\mathrm{xc},\alpha}, \tag{7}$$

where four components are defined by

$$\varepsilon_{\mathrm{rk},\alpha} = -\left\langle\alpha\left|\frac{1}{r^2}\frac{\partial}{\partial r}\left(r^2\frac{\partial}{\partial r}\right)\right|\alpha\right\rangle, \tag{8}$$

$$\varepsilon_{\mathrm{cp},\alpha} = l(l+1)\left\langle\alpha\left|1/r^2\right|\alpha\right\rangle, \tag{9}$$

$$\varepsilon_{\mathrm{H},\alpha} = \left\langle\alpha\left|V_{\mathrm{H}}{}^{\alpha}\right|\alpha\right\rangle, \tag{10}$$

and

$$\varepsilon_{\mathrm{xc},\alpha} = \left\langle\alpha\left|V_{\mathrm{xc}}{}^{\alpha}\right|\alpha\right\rangle. \tag{11}$$

The first two components $\varepsilon_{\mathrm{rk},\alpha}$ and $\varepsilon_{\mathrm{cp},\alpha}$ add up to the total kinetic energy $\varepsilon_{\mathrm{k},\alpha}$.

3. Results and discussion

Having fixed the outer radius R_2 and the spread-out ion density ρ_0 of the JS, we vary the electron number N and the inner radius R_1 of the JS simultaneously under the charge-neutrality condition of the whole system. The outer radius R_2 is taken to be $R_2=20.67$ in atomic units, and the fixed ion density ρ_0 corresponds to the density parameter $r_{s0}=(3/4\pi\rho_0)^{1/3}=4$. When $R_1=0$, our system becomes a solid jellium sphere in which 138 electrons have a closed-shell configuration. With increase of R_1, we follow the variation of the electronic structure from a solid sphere to a spherical layer sharply localized in the radial direction.

Figure 1 displays the variation of the electronic structure with increase of R_1. The results in the SIC-LDA scheme are compared with those in the ordinary LDA scheme. Three full curves and three dotted curves in each upper panel of Figs. 1(a)-1(d) indicate the radial dependence of $V_{\mathrm{H}}{}^{(0)}$, $V_{\mathrm{xc}}{}^{(0)}$ and $V_{\mathrm{eff}}{}^{(0)}$ in the SIC-LDA scheme and in the ordinary LDA scheme, respectively. The effective potential $V_{\mathrm{eff}}{}^{(0)}$ is given by

$$V_{\mathrm{eff}}{}^{(0)}(\boldsymbol{r}) = V_{\mathrm{H}}{}^{(0)}(\boldsymbol{r}) + V_{\mathrm{xc}}{}^{(0)}[\rho(\boldsymbol{r})], \tag{12}$$

and $V_{\mathrm{H}}{}^{(0)}$ is already defined in eq. (5). A full curve and an unlabeled dotted curve in each lower panel of Figs. 1(a)-1(d) exhibit the electron density distribution in the SIC-LDA scheme and in the ordinary LDA scheme, respectively. Broken lines signify the spread-out ion density of the JS. Dotted curves labeled with l as s, p, d, $\cdots$ indicate the decomposition of the electron density distribution into constituent l components, and some of these curves include more than one electron shell. Each electron shell is specified by n and l, often in the form of nl, and energy levels of electron shells for each l are numbered by $n(=1, 2, 3, \cdots)$ in order of increasing energy. Figures 2(a)-2(d) indicate energy levels of occupied electron shells for four

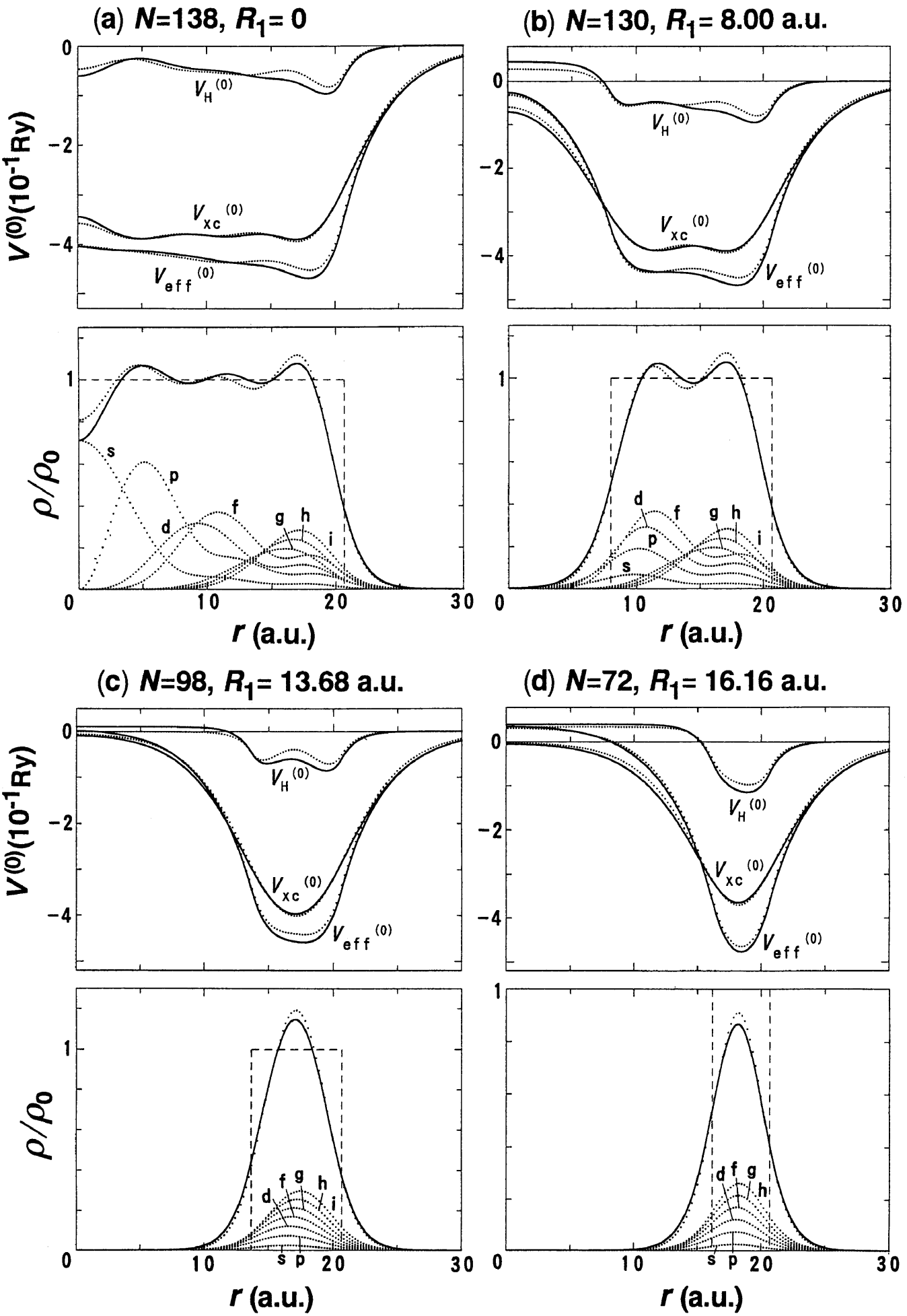

Figure 1. Electronic structure of four spherical jellium shells with R_2=20.67 a.u. and r_{s0}=4. Electrons in each system have a closed-shell configuration. Adapted from Fig. 1 in ref. 10.

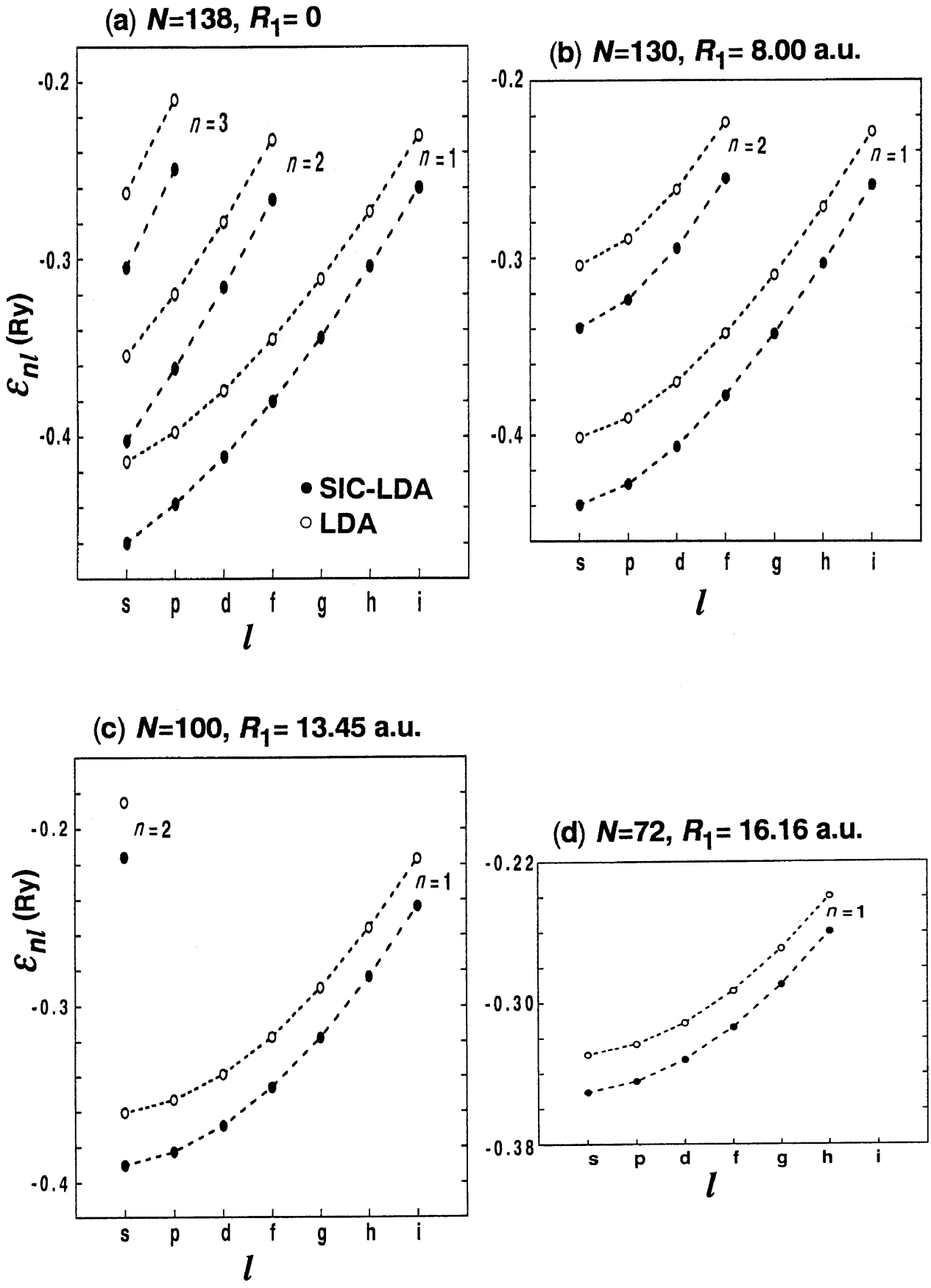

Figure 2. Energy levels of occupied electron shells of four spherical jellium shells with R_2=20.67 a.u. and r_{s0}=4. Full and open circles represent the results with and without the SIC, respectively. Adapted from Fig. 3 in ref. 10.

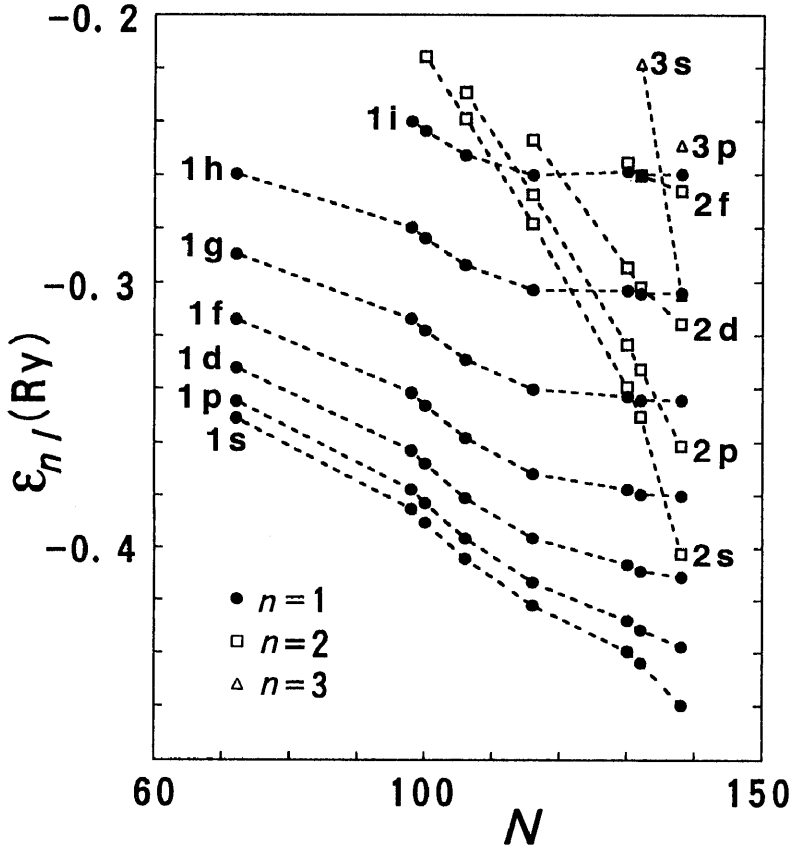

Figure 3. Variation of occupied electron-shell levels with change in size of the hollowed-out core. Adapted from Fig. 4 in ref. 10.

JS's in the SIC-LDA scheme (full circles) and in the ordinary LDA scheme (open circles). The energy-level points for each number n are connected by broken lines. The panels (a), (b) and (d) in Fig. 2 corresponds to panels (a), (b) and (d) in Fig. 1, respectively. Figure 3 displays the shift of energy levels of occupied electron shells with change of R_1 in the SIC-LDA scheme. A series of energy-level points for each electron shell are connected by broken lines.

When N=132, the 3s shell is closed and the 1j shell is empty, as exhibited in Fig. 3. If we assume this electron configuration and perform a self-consistent calculation in the ordinary LDA scheme, we obtain an incorrect solution where the occupied 3s level is slightly higher than the empty 1j level. The reason why we can obtain a correct solution in the SIC-LDA scheme is that the SIC operates to lower occupied energy levels, and consequently the 3s level becomes lower than the 1j level.

First, we pay attention to characteristics of shell density distributions $\rho_{nl}(r)$, namely, shell components in the electron density distribution, in the jellium sphere with N=138. As exhibited in the lower panel of Fig. 1(a), the s and p components in the electron density distribution have their substantial intensity around or near the center, while the g, h and i components, which involve only the 1g, 1h and 1i shells, respectively, are well localized near the surface. The s and p components are decomposed into ns- and np-shell components (n=1, 2, 3) in Figs. 2(a) and 2(b) in ref. 10. What is characteristic of the jellium sphere is that the shell density distribution $\rho_{nl}(r)$ varies remarkably with angular momentum l for each number n. This variation is most outstanding in the 1l shells. As a centrifugal potential operates more strongly with increase of l, an electron shell transfers its substantial probability density remarkably to an outer region, and has its probability density more concentrated in the radial direction.

Next, we examine the variation of the electronic structure with increase in size of the hollowed-out core. Figure 3 implies that with increase of R_1, the shell levels with $n \geq 2$ ascend quickly, passing through the occupied shell levels with n=1, and become empty. This is manifest in Fig. 2 also. By following the series of Fig. 2(a)-2(d), we notice that the variation of shell-level occupation is analogous to the thickness dependence of subband occupation of an electron system in the film. A series of shell levels for each n can be regarded as a subband in the film electron system. With decrease of the film thickness, subbands become further separated from one another in energy, less and less subbands become occupied, and finally the lowest subband remains occupied.

Here, we examine the variation of shell density distributions $\rho_{nl}(r)$. As a core is hollowed out with decrease of N, electron shells with lower l such as ns and np shells make a great outward shift of their probability density, and have their probability density more localized in the radial direction. In sharp contrast to this remarkable change, the presence of the hollowed-out core has no significant influence on electron shells with higher l such as the 1g, 1h and 1i shells, because originally these electron shells have their concentrated probability density in an outer region near the external edge of the JS (see the g, h and i components in $\rho(r)$ in each lower panel of Figs. 1(a)-1(d)). When N=98, only the electron shells with n=1 remain occupied, and an electron shell with higher l has its probability density somewhat more concentrated in a somewhat

outer region (see Fig. 1(c)). With further decrease of N to 72, eigenfunctions of occupied orbitals with n=1 take almost the same radial dependence regardless of l, and each expectation value in eqs. (8)-(11) becomes almost independent of l. Consequently, each occupied $1l$ shell takes almost the same probability density distribution irrespective of l, apart from a proportionality constant (see the lower panel of Fig. 1(d)), and its energy level varies as $l(l+1)$, aside from an additive constant (see Fig. 2(d)). This energy-level variation is the same as in an electron system confined on a spherical surface. As suggested in Fig. 1(d), these characteristics in the final stage are well established when the JS becomes so thin that a considerable fraction of the electron density penetrates into the vacuum and the maximum of the electron density becomes lower than the ion density level of the JS. We can put the above variation briefly as follows: in the jellium sphere, an nl shell with higher l has its substantial probability density in an outer region and has its probability density more concentrated in the radial direction. As the hollowed-out core becomes larger, an electron shell originally having its radially extended probability density in an inner region undergoes a larger intensity shift of its probability density to an outer region and a greater variation in radial localization of its probability density, and in the final stage, all the occupied $1l$ shells take almost the same probability density distribution irrespective of l.

As exhibited in Fig. 3, energy levels of occupied electron shells tend to increase, as the bored core becomes larger. This energy increase can be examined by decomposing an eigenenergy ε_α into four components, as defined in eqs. (7)-(11). As typical examples, figure 4 shows the energy variation of $1p$ and $2p$ orbitals and its decomposition into four components. The symbols 'k', 'rk', 'cp', 'H' and 'xc' signify $\varepsilon_{k,\alpha}$, $\varepsilon_{rk,\alpha}$, $\varepsilon_{cp,\alpha}$, $\varepsilon_{H,\alpha}$ and $\varepsilon_{xc,\alpha}$, respectively. Note the relation $\varepsilon_{k,\alpha}=\varepsilon_{rk,\alpha}+\varepsilon_{cp,\alpha}$. The three components $\varepsilon_{xc,\alpha}$, $\varepsilon_{H,\alpha}$ and $\varepsilon_{rk,\alpha}$ cooperate to increase ε_α as the hollowed-out core becomes larger, except that $\varepsilon_{H,1p}$ operates to decrease ε_{1p} when N drops from 98 to 72. On the other hand, the component $\varepsilon_{cp,\alpha}$ operates against $\varepsilon_{rk,\alpha}$ to decrease ε_α, and consequently the total kinetic energy $\varepsilon_{k,\alpha}$ makes a reduced contribution to the increase of ε_α.

The XC effects are taken into account within the LDA, and the XC potential $V_{xc}^{(0)}$ decreases at higher electron density (see Fig. 1). The SIC potential V_{xc}^{α} can be obtained by subtracting the self-interaction contribution of orbital α from $V_{xc}^{(0)}$ (see eq. (6)). The potential curve of V_{xc}^{α} still retains the well form, though the SIC causes a considerable upward shift from $V_{xc}^{(0)}$ to V_{xc}^{α} where ρ_α is higher. In the jellium sphere or in a thick JS, an orbital with lower l has a greater part of its density profile curve embedded in a higher electron-density region well inside the jellium sphere or the JS. This character of the orbital density distribution lowers the XC component $\varepsilon_{xc,\alpha}$. However, as our electron system becomes more localized in the radial direction with increase of R_1, the orbital starts to extend a larger part of its density profile curve to a lower electron-density region at the inner or outer surface. This process gives rise to the increase of $\varepsilon_{xc,\alpha}$.

The increase of $\varepsilon_{H,\alpha}$ can be understood in the same manner, The potential V_H^{α} has a well-shaped profile curve as $V_H^{(0)}$ which bends up at the inner or outer surface, though the curve of V_H^{α} lies considerably below that of $V_H^{(0)}$ because of subtraction of the self-interaction contribution. Therefore, the component $\varepsilon_{H,\alpha}$ increases with increase of R_1, because the orbital extends a larger part of its density profile curve to the surface region where V_H^{α} turns up. However, this can not explain the decrease of $\varepsilon_{H,1p}$ when N falls from 98 to 72. When N decreases from 98 to 72, the potential curve V_H^{α} of each occupied $1l$ orbital varies its form from a double-minimum to a single-minimum well and the potential well becomes deeper, because at N=72 a considerable fraction of the electron density penetrates into the vacuum and the peak of the electron density becomes lower than the ion density level of the JS (see Figs. 1(c) and 1(d)). This variation of V_H^{α} lowers $\varepsilon_{H,\alpha}$ of each $1l$ orbital which has its substantial orbital density in the potential well.

As the hollowed-out core becomes larger, the radial kinetic energy $\varepsilon_{rk,\alpha}$ increases because our electron system becomes more localized in the radial direction, while the centrifugal potential energy $\varepsilon_{cp,\alpha}$ decreases because an orbital with its definite angular momentum l shifts its probability density to an outer region (see eq. (9)). When l is lower, the contribution of $\varepsilon_{rk,\alpha}$ to variation of ε_α predominates over that of $\varepsilon_{cp,\alpha}$, as shown in Fig. 4.

Here, we examine the ionization potential (IP) of our JS systems. In the SIC-LDA scheme, we can make a good estimate of the IP by the absolute value of the highest energy level of occupied orbitals. Accordingly, we can evaluate the IP for a series of JS's with closed-shell configurations by following the highest energy level of occupied electron shells in Fig. 3. In view of the size dependence of the IP in jellium spheres including open-shell configurations (see refs. 13-16), we can expect a saw-tooth variation of the IP due to the electron-shell structure for our JS systems also. The variation of the IP with increase of R_1 indicates the transition of the highest occupied shell in the order of $3p, 3s, 2f, 2d, 2p, 2s, 1i, 1h, \cdots$. Therefore, this variation of the IP involves the quick ascent of shell levels with $n \geq 2$ which is characteristic of our JS systems.

Finally, we compare the results in the SIC-LDA scheme with those in the ordinary LDA scheme. The SIC causes a considerable downward shift of occupied energy levels (see Fig. 2), though it makes no significant difference in the electron density distribution ρ and in the potentials $V_H^{(0)}$, $V_{xc}^{(0)}$ and

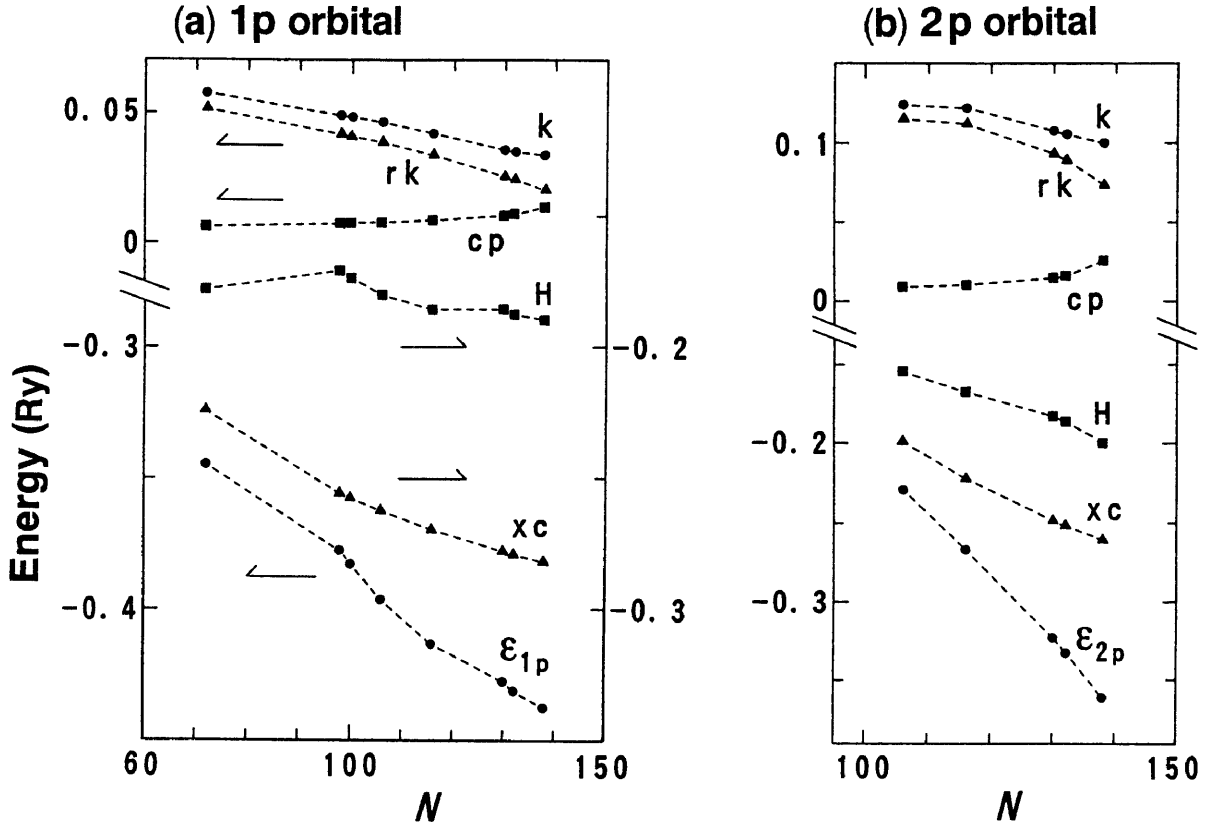

Figure 4. $1p$- and $2p$-orbital energies, ε_{1p} and ε_{2p} , and their decomposition into $\varepsilon_{\mathrm{rk},np}$, $\varepsilon_{\mathrm{cp},np}$, $\varepsilon_{\mathrm{H},np}$ and $\varepsilon_{\mathrm{xc},np}$ (n=1,2) for a series of spherical jellium shells. Each arrow in panel (a) appoints a scale on the left or right side relevant to a series of points. Adapted from Fig. 6 in ref. 10.

$V_{\mathrm{eff}}^{(0)}$ (see Fig. 1). The SIC components in $\varepsilon_{\mathrm{H},\alpha}$ and $\varepsilon_{\mathrm{xc},\alpha}$ can be expressed as

$$\Delta\varepsilon_{\mathrm{H},\alpha} = -2\int \mathrm{d}^3r \int \mathrm{d}^3r' \frac{\rho_\alpha(r)\rho_\alpha(r')}{|r-r'|}, \qquad (13)$$

and

$$\Delta\varepsilon_{\mathrm{xc},\alpha} = -\int \mathrm{d}^3r \rho_\alpha(r) V_{\mathrm{xc}}^{\mathrm{P}}[\rho_\alpha(r)], \qquad (14)$$

respectively (see eqs. (5), (6), (10) and (11)). The former $\Delta\varepsilon_{\mathrm{H},\alpha}$ operates to decrease ε_α because it is negative, while the latter $\Delta\varepsilon_{\mathrm{xc},\alpha}$ acts to increase ε_α because it is positive. However, the former is more influential than the latter, which results in the downward shift of each occupied energy level. Here, we focus our attention on the l dependence of this downward energy shift in a series of orbitals for each n. In the jellium sphere, an orbital with lower l has larger values of $|\Delta\varepsilon_{\mathrm{H},\alpha}|$ and $\Delta\varepsilon_{\mathrm{xc},\alpha}$, because a normalized orbital with lower l has its substantial density in a smaller r range, which gives higher orbital density there (see eqs. (13) and (14)). Note that the XC potential $V_{\mathrm{xc}}^{\mathrm{P}}[\rho_\alpha]$ decreases at higher orbital density ρ_α. The negative component $\Delta\varepsilon_{\mathrm{H},\alpha}$ makes more contribution to the l dependence of ε_α than the positive component $\Delta\varepsilon_{\mathrm{xc},\alpha}$. Consequently, an orbital energy ε_α with lower l makes a greater downward shift due to the SIC, though it is not so remarkable because $\Delta\varepsilon_{\mathrm{xc},\alpha}$ operates against $\Delta\varepsilon_{\mathrm{H},\alpha}$ (see Fig. 2(a)). With increase of R_1, an orbital with lower l suffers a greater intensity shift of its probability density to an outer region, and eventually all the occupied $1l$ orbitals take almost the same radial dependence in their probability density distributions. Along with this evolution of orbital density distributions, the l dependence of the downward energy shift becomes smaller, and finally all the occupied $1l$ orbitals make almost the same energy shift regardless of l (see Fig. 2(d)).

4. Summary

The electronic structure of the jellium sphere can be characterized by the remarkable l dependence of the shell density distribution ρ_{nl} for each n. Because of a stronger centrifugal potential, an occupied electron shell with higher l has its substantial probability density in an outer region, which is more localized in the radial direction. As the hollowed-out core becomes larger, the electronic structure varies as follows:

(a) The occupied shell levels with $n \geq 2$ ascend rapidly and become empty one after another. This change of shell-level occupation is analogous to the thickness dependence of subband occupation in a film electron system. This shell-level change should be reflected in the variation of the ionization potential.

(b) In a sequence of occupied electron shells for each n, a shell with lower l initially having more extended probability density in an inner region of the jellium sphere suffers a larger intensity

shift of its probability density to an outer region and a greater variation in radial localization of its probability density.

(c) In a series of occupied shell levels for each n, a level with lower l increases more significantly, because its shell is more seriously influenced by the increase in size of the hollowed-out core, as mentioned in (b). This level increase can be analyzed by decomposing each orbital energy into the radial kinetic, the centrifugal, the electrostatic and the XC part.

After passing through the above process, we reach a sharply localized electron system where all the occupied shells with n=1 take almost the same probability density distribution independent of l, and the occupied shell level ε_{1l} varies as $l(l+1)$ apart from an additive constant. Such a sharply localized system is well established when the thickness of the JS becomes close to the electron penetration length at the surface, and a considerable fraction of the electron density penetrates into the vacuum. The above l dependence of ε_{1l} is the same as in an electron system confined on a spherical surface.

Secondly, we have investigated effects of the SIC by comparing the results in the SIC-LDA scheme with those in the ordinary LDA scheme.

(a) The SIC lowers each occupied shell level significantly. We have obtained a correct self-consistent solution in the SIC-LDA scheme for a delicate case also (N=132) where one of two very close shell levels is occupied and the other is empty.

(b) We have analyzed the l dependence of the downward energy shift due to the SIC in a series of occupied shell levels for each n. In a jellium sphere or in a thick JS, an electron shell with lower l makes a greater downward shift of its energy level. As the hollowed-out core becomes larger, this l dependence of the downward shift of the shell level becomes less outstanding, and in a sharply localized system, all the occupied $1l$ shells make almost the same energy shift regardless of l.

Acknowledgements

The author would like to express his thanks to M. Hasegawa for valuable discussions. He is grateful to H. Ojima for help in preparing the manuscript and figures. This work was supported by a Grant-in-Aid for Scientific Research from the Ministry of Education, Science and Culture, No. 04640359. Numerical calculations in this work were performed at the Iwate University computer center.

1) A. A. Lushnikov, V. V. Maksimenko and A. J. Simonov, Z. Phys. B **27** (1977) 321.
2) R. Rojas, F. Claro and R. Fuchs, Phys. Rev. B **37** (1988) 6799.
3) L. Genzel, T. P. Martin and U. Kreibig, Z. Phys. B **21** (1975) 339.
4) H. S. Zhou, I. Honma, H. Komiyama and J. W. Haus, Phys. Rev. B **50** (1994) 12052.
5) T. Inaoka, J. Phys. Soc. Jpn. **62** (1993) 1692.
6) J. W. Haus, H. S. Zhou, S. Takami, M. Hirasawa, I. Honma and H. Komiyama, J. Appl. Phys. **73** (1993) 1043.
7) T. Inaoka, J. Phys. Soc. Jpn. **63** (1994) 2490.
8) K. Kawamura, N. Urata and M. Eto, in *Proceedings of 7th International Symposium on Small Particles and Inorganic Clusters* (World Scientific, Kobe, 1994).
9) M. Eto and K. Kawamura, Phys. Rev. B **51** (1995) 10119.
10) T. Inaoka, J. Phys. Soc. Jpn. **64** (1995) 1658.
11) H. W. Kroto, J. R. Heath, S. C. O'Brien, R. F. Curl and R. E. Smalley, Nature (London) **318** (1985) 162.
12) see, e.g., K. Yabana and G. F. Bertsch, Phys. Scripta **48** (1993) 633.
13) W. Ekardt, Phys. Rev. B **29** (1984) 1558.
14) D. E. Beck, Solid State Commun. **49** (1984) 381.
15) M. J. Puska, R. M. Nieminen and M. Manninen, Phys. Rev. B **31** (1985) 3486.
16) Y. Ishii, S. Ohnishi and S. Sugano, Phys. Rev. B **33** (1986) 5271.
17) W. D. Knight, K. Clemenger, W. A. de Heer, W. A. Saunders, M. Y. Chou and M. L. Cohen, Phys. Rev. Lett. **52** (1984) 2141.
18) W. D. Knight, *The Chemical Physics of Atomic and Molecular Clusters,* ed. G. Scoles (North-Holland, Amsterdam, 1990) p. 413.
19) J. P. Perdew and A. Zunger, Phys. Rev. B **23** (1981) 5048.
20) W. Kohn and L. J. Sham, Phys. Rev. **140** (1965) A1133.
21) D. M. Ceperley and B. J. Alder, Phys. Rev. Lett. **45** (1980) 566.